Computers and Chemical Engineering 140 (2020) 106870

Contents lists available at ScienceDirect

Computers and Chemical Engineering

journal homepage: www.elsevier.com/locate/compchemeng

Surrogate based optimization of a process of polycrystalline silicon production

César Ramírez-Márquez[a], Edgar Martín-Hernández[b], Mariano Martín[b,*], Juan Gabriel Segovia-Hernández[a]

[a] Universidad de Guanajuato, Campus Guanajuato, División de Ciencias Naturales y Exactas, Departamento de Ingeniería Química, Noria Alta S/N, 20256, Guanajuato Gto., México
[b] Universidad de Salamanca, Departamento de Ingeniería Química. Plza.Caídos 1-5, 37008, Salamanca, España

ARTICLE INFO

Article history:
Received 15 December 2019
Revised 6 March 2020
Accepted 15 April 2020
Available online 25 May 2020

Keywords:
Process of polycrystalline silicon production
Optimal operating conditions
High production of polycrystalline

ABSTRACT

A hybrid polycrystalline silicon production route is optimized following a two-step procedure. First, surrogate models for the main units are developed following different techniques which depend on the available information. Secondly, the optimization of the entire process flowsheet allows determining the optimal tradeoff between yield and energy consumption. A base production capacity of 2000 t/y of polycrystalline silicon is considered, with an equipment cost of 9.97 M$. Three scenarios are evaluated: maximum silicon production, minimum operating costs and maximum total profit. The maximization of the total profit is the most promising scenario, obtaining a selling price of 8.93 $/kg$_{Poly}$, below the commercial price, 10 $/kg$_{Poly}$. The revenue obtained is 10 M$/y, with an operating cost of 6.48 M$/y. Furthermore, a plant scale-up study was performed. If the production capacity is increased by a factor of 10, it results in a reduction of 1.03 $/kgSi$_{Poly}$.

1. Introduction

Climate change is one of the major concerns of our society. Some of the effects of the climate change represent a threat for the survival of many human communities due to the rise of the sea level, food shortages as a result of poor crops, and water scarcity, among other consequences. To address this challenge and cope with the increasing global energy consumption, changes in our production system must be addressed. One of the main challenges is the generation of energy through ecological and sustainable paths. Among the most promising alternatives with the potential to meet these requirements are solar energy and silicon-based solar cells (Green, 2009).

Although silicon-based photovoltaic panels can be built using both polycrystalline and monocrystalline silicon, the scope of this work focuses on polycrystalline technologies. Traditionally, polycrystalline silicon (also called polysilicon), has been used in the microelectronic industry (Pizzini, S., 2010). However, the rise of the solar power sector in the last decade turned the photovoltaic industry (PV) into the main consumer of polysilicon (Hesse et al., 2009). As a result, the polysilicon production has been surpassed by the demand generated from the photovoltaic industry, creating a shortage of supply (Chigondo, 2018). Additionally, the development of the PV industry has led to a decrease in the generation cost of electricity, allowing some countries to reach the socket parity (Polman et al., 2016). However, further reductions in the cost of photovoltaic cells and increases in the electricity production efficiency are needed to improve the competitiveness the solar-based electricity, ensuring its long-term sustainability, and its expansion into new markets (Wang et al., 2013; Morita & Yoshikawa, 2011). Since approximately one half of the finished module costs relies on the production of polycrystalline silicon (Weber et al., 2004), reducing the manufacturing cost of polysilicon is a key objective to reduce the manufacturing cost of solar panels.

Two silicon production processes are widely used: the metallurgical process to produce silicon at purity of 98-99%, and the chemical path to further increase the purity reaching solar grade silicon (SG-Si) (Ranjan et al., 2011; Zadde et al., 2002). Industrial production of SG-Si using metallurgic routes is under development. There are two industrial processes that can be distinguished within the chemical route: the Siemens process, based on the decomposition of trichlorosilane at high temperature in a hydrogen atmosphere ($SiHCl_3$) (O'Mara et al., 2007; Nie et al., 2018), and the process developed by Union Carbide Co., based on the disproportion of trichlorosilane to produce silane (SiH_4) as high purity silicon precursor of polysilicon (Union Carbide, 1981).

* Corresponding author.
E-mail address: mariano.m3@usal.es (M. Martín).

https://doi.org/10.1016/j.compchemeng.2020.106870
0098-1354/

Nomenclature

w	Total number of elements in the system
p	Price of each by-product *SP [$/unit]*
k	Overall constant reaction
$d\,MO$	Cost of manpower [$/unit]
c	Cost of each utility *E [$/unit]*
b	The unit cost of each raw material *RM [$/unit]*
a	Factor that considers annual expenses such as maintenance [$/unit]
W	Work exchanged by the system [J]
Q	Heat exchanged by the system [J]
z	Polytropic coefficient
x	Mole fraction
X	Amount of the species [mass fraction]
TAC	Total Annual Cost [$/y]
T	Temperature [K]
SiO_2	Silicondioxide
SiO	Silicon oxide
Si_{MG}	Metallurgical grade silicon
$SiHCl_3$	Trichlorosilane
SiH_4	Silane
SiH_2Cl_2	Dichlorosilane
$SiCl_4$	Silicontetrachloride
SiC_2	Silicondicarbide
SiC	SiliconCarbide
Si_2C	DisiliconCarbide
Si_2	Disilicon
Si	Silicon
RR	Reflux Ratio
ROI	Return on investment
Rel	$H_2/SiCl_4$ molar feed ratio
R	Molar gas constant
PV	Photovoltaic
P	Pressure [kPa]
NLP	Nonlinear program
N	Number of species in the reaction system
IR	Individual Risk
HCl	Hydrogen chloride
H_2	Hydrogen
GAMS	General Algebraic Modeling System
FR	Feed Ratio
FBR	Fluidized Bed Reactor
EI99	Eco-indicator 99
CO	Carbon monoxide
C	Carbon
ΔH	Enthalpy variation [J/mol]
μ_i	Viscosity of the species *i[Pa·s]*
μ_i	Chemical potential [J/mol]
v_i	Stoichiometry coefficients of involved compounds
n_i	Amount of the component i [mol]
n_c	Efficiency of the compressor
k_r	Rate of decomposition.
k_{ad}	Rate of $SiHCl_3$ chemisorption on the surface
f_i^o	Standard fugacity of species i [kPa]
$fc_{polycrystalline\,silicon}$	Mass flow of polycrystalline silicon [kg/s]
a_{ik}	Number of k_{th} atoms in each molecule of species i
$W_{(Compressor)}$	Electrical energy [kW]
V_{SiMG}	Molar volume of silicon [m^3/mol];
$T_{outCompressor}$	Out temperature [K];
$T_{inCompressor}$	Entry temperature [K];
T_{RebCol}	Bottom temperature [K]
T_{ConCol}	Top temperature [K]
$S_{polycrystalline\,silico}$	Profit from the sale of the polycrystalline siliconde
S_i^o	Standard entropy [J/K·mol]
Q_{RebCol}	Reboiler heat duty [kW]
Q_{ConCol}	Condenser heat duty [kW]
$P_{outCompressor}$	Out pressure [kPa]
P^o	Standard-state pressure (100 kPa);
$P_{inCompressor}$	Entry pressure [kPa]
I_F	Fixed annualized investment [$]
H_i^o	Standard enthalpy [J/mol]
H_{fi}^{Tref}	Standard enthalpy for each element *i [J/mol]*
G_i^o	Standard Gibbs free energy [J/mol]
G^T	Total Gibbs free energy [J]
C_{pi}	Specific heat of the component i [J/molK]
$C_{p,\,i}$	Heat capacity [J/molK]
A_K	Total atomic mass of the k_{th} element in the system
R_i	Mass rate of change in species *i* by chemical reaction
ΔE_P	Variation of potential energy [J]
ΔE_C	Variation of kinetic energy [J]
$\widehat{\varphi}_i$	Fugacity coefficient
$\widehat{f}_i$	Fugacity [kPa]
λ_i	Specific latent heat for each element *i [J/mol]*
y_i	Molar fraction of species i

To achieve the targets of lower manufacturing costs and higher production capacity, novel processes are needed. In previous works, Ramírez-Márquez et al. (2018, 2019), a process with high production capacity of polycrystalline silicon has been developed and optimized using different objective functions: economic (total annual cost (TAC) and the return on investment (ROI)), safety (the individual risk index (IR)), and environmental (eco-indicator 99 (EI99)). The optimization was carried out using a stochastic optimization scheme within the Aspen Plus® software. Although Aspen Plus® contains several modules for reactors simulation, the definition of custom models is not feasible, preventing the use of a specific model for the reaction system evaluated. As a result, one of the observed drawbacks of the methodology used is the impossibility of evaluating the operating conditions of the reaction systems. Thus, only the separation systems are optimized.

There are a number of works which individually describe the different units of the process. Yadav et al. (2017) reviewed numerical models incorporating thermodynamics, reaction kinetics, fluid dynamics, heat and mass transfer calculations to examine the refinement of metallurgical silicon to polycrystalline silicon production for each unit independently. The hydrogenation of trichlorosilane in a fixed bed reactor has been studied by Sugiura et al. (1992). Likewise, Kato and Wen (1969) tested models for gas-solid fluidized beds, developing models based on a three-phase theory involving bubble, emulsion and cloud phases. Wang (2011) conducted a study of 2-D cylindrical fluidized bed reactor model for hydrochlorination of silicon. Ni et al. (2014) presented studies of gas velocity distribution in bell-jar reactor with 12 rods of three different diameters from 3-D CFD simulations. Although there are a number of works which independently describe the units of the polycrystalline silicon production process, there is

no study that captures the features of all the major units within a process model.

Here, the major units of the process, not only distillation columns but specially the reactors, involved in the production of silicon polycrystalline are modeled based on experimental and industrial data. Different surrogate modeling approaches are used depending on the data available to develop a framework for the entire process for polycrystalline silicon production in Ramírez-Márquez et al. (2018) that will allow evaluating the operating conditions at each of the units towards minimizing the production cost of the polycrystalline silicon.

Surrogates are useful to execute difficult calculations (Fahmi and Cremaschi, 2012). Several authors have proposed the use surrogate models in engineering design to treat significant aspects such as global optimality (Audet, et al., 2000; Henao and Maravelias, 2010). Amongst the popular techniques to produce such surrogates we find Kriging and Artificial Neural Networks (ANN) (Voutchkov, and Keane, 2006). Caballero and Grossmann (2008) have applied Kriging-based models to the solution of special classes of the synthesis-optimization of chemical process. The literature review also presents numerous works applying ANNs to process modeling and optimization (Henao and Maravelias, 2010; Fahmi and Cremaschi, 2012; Schweidtmann et al., 2019).

The process proposed can be divided into four main sections. The first stage is the carboreduction of SiO_2 using C to obtain metallurgical silicon. The second section corresponds to the production of chlorosilanes through the reactions system formed by the hydrogenation of silicon tetrachloride and the hydrochlorination of metallurgical silicon with HCl. The third step consists in the purification of the chlorosilanes obtained from the previous reactor using distillation columns. Finally, the fourth section is the conversion of trichlorosilane into polysilicon in a Siemens deposition reactor. The entire process is modeled as a Non Linear Programing (NLP) problem.

The rest of the paper is organized as follows. Section 2 describes the process studied. Section 3 shows the development of surrogate models for all units. In Section 4 the solution procedure presenting the various objective functions is discussed. Section 5 comments on the results and, finally, conclusions are drawn.

2. Methodology for process design

To be able to compare the results obtained with the performance of current polysilicon plants, a facility with a capacity of 2,000 ton/year of polycrystalline silicon, similar to current industrial polysilicon plants (Nitol Chem Group 1,500 ton/year, PV Crystalox 2,250 ton/year, SolarWorld, 3,200 ton/year) (List of World's Polysilicon Producers According to Country for Last 3) has been considered.

With the aim to reduce the manufacturing costs of the photovoltaic panels, mainly driven by the silicon cost, a hybrid polycrystalline silicon production route combining the stages of Siemens and Union Carbide with better performance was developed in previous work in order to reduce the manufacturing costs of the polysilicon cost (Ramírez-Márquez et al., 2018).

The Siemens process, shown in Fig. 1, is based on the use of trichlorosilane ($SiHCl_3$) as silicon source. $SiHCl_3$ is obtained from a process which starts from the reduction of quartz in an electrical arc furnace, obtaining metallurgical grade silicon (Si_{MG}). The Si_{MG} produced reacts with hydrogen chloride (HCl) in a fluidized bed reactor (FBR) to produce a gas stream composed of a mixture of chlorosilanes. Among them, the most important is trichlorosilane, which will be used as precursor in the polysilicon production stage (Pazzaglia et al., 2011). Subsequently, the purification process

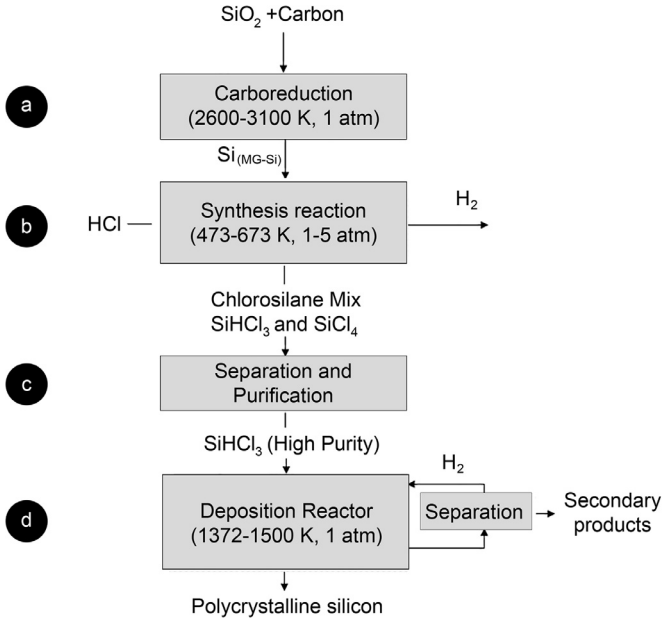

Fig. 1. Siemens process flow diagram (Ramirez-Marquez et al., 2018).

consisting of a distillation column sequence is used to obtain ultrapure trichlorosilane. Finally, in the polycrystalline silicon production, the ultrapure trichlorosilane is decomposed in a chemical vapor deposition reactor known as Siemens reactor (Erickson & Wagner, 1952). It should be noted that a relevant drawback of the Siemens process is the need of use extremely pure HCl for the synthesis of chlorosilanes, with the safety and environmental risks inherent to the use of this compound.

On the other hand, the process developed by Union Carbide Co., shown in Fig. 2, uses silane (SiH_4) as a source of polycrystalline silicon. As in the case of the Siemens process, Si_{MG} is produced via metallurgical reduction of SiO_2 and C. Both Si_{MG} and silicon tetrachloride (which is recirculated from the following step) are hydrogenated in a fluidized bed reactor to produce chlorosilanes: $SiCl_4$, SiH_2Cl_2, and $SiHCl_3$ (Iya, 1986). Subsequently, the separation and purification of chlorosilanes are performed. The trichlorosilane can be transformed into silane through successive redistribution reactions (Iya, 1986), or through the use of reactive distillation columns (Muller et al., 2002; Ramírez-Márquez et al., 2016). Finally, the high purity silane obtained is introduced into a vapor deposition reactor where it is decomposed to produce the polycrystalline silicon. The Union Carbide Co. process achieves higher efficiencies since the conversion of silane to silicon is larger than the trichlorosilane transformation to silicon used in the Siemens process. However, this process operates under more extreme conditions to those used in the Siemens process.

From the process descriptions above, it can be observed that the conventional processes for polycrystalline silicon production can be divided into four main stages: a) thermal carboreduction stage, where a metallurgical reduction is carried out. This process consists of melting the silica in presence of carbon in an electric arc furnace at a temperature above of the boiling point of SiO_2 (2773.15 K) to produce Si_{MG}; b) chlorosilanes production from Si_{MG} in fluidized bed reactors; c) the purification stage, that separates different chlorosilanes originated from the previous process; and finally d) polycrystalline silicon production through chemical vapor deposition. Considering every stage of the conventional processes, the process for polycrystalline silicon production shown in Fig. 3 was developed by the Ramírez-Márquez et al. (2018 & 2019). In those works, the conceptual design of the process, named as Hy-

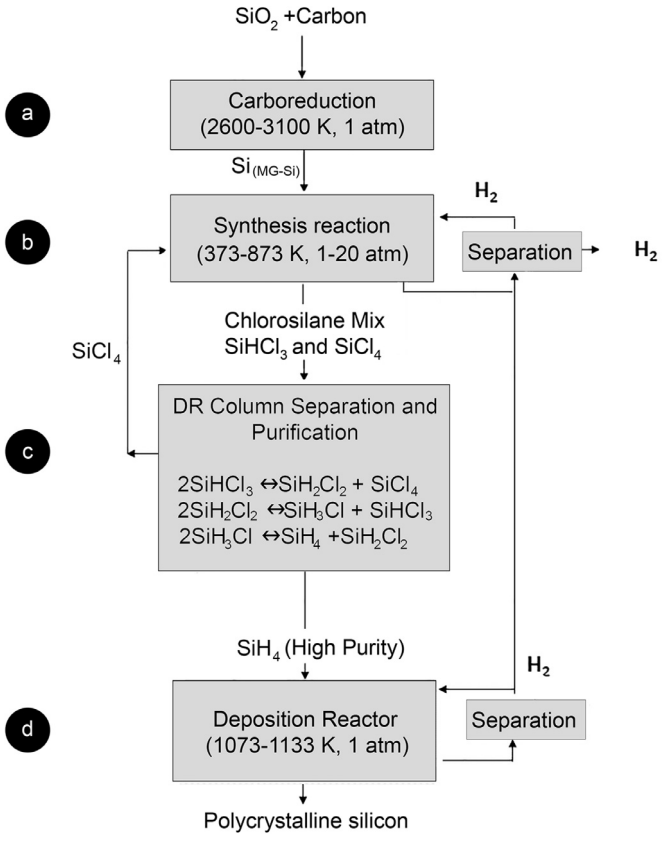

Fig. 2. . Union Carbide Co. process flow diagram (Ramírez-Márquez et al., 2018).

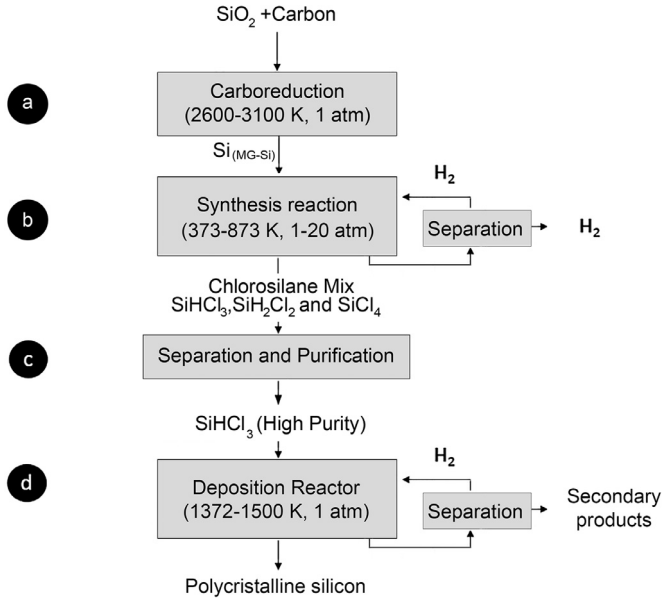

Fig. 3. Hybrid process flow diagram (Ramírez-Márquez et al., 2018).

brid Process, is carried out through the strategic combination of stages of the Siemens process and the Union Carbide Co. process. The conceptual design was driven by the idea of taking advantage of the maximum productivity of each stage, combining them in the optimal arrangement, and verifying the feasibility of the final integration of stages.

As shown in Fig. 3, the first stage of the Si_{MG} production is carried out similarly in both conventional processes through the metallurgical reduction of SiO_2 with C. The global reaction of quartz reduction in the arc furnace is the detachment of the oxygen from the SiO_2, which is captured by C to form carbon monoxide (CO). However, the carboreduction process in the reactor, carried out at a temperature above the SiO_2 boiling point (2773.17 K) is more complicated, generating other by-products such as SiC(s), Si_2C(g), Si_2(g), SiC_2(g), Si(g) and SiO(g). Therefore, in this work a more detailed model for the reaction considering the distribution of species of the system Si-O-C is developed as a function of the temperature (Wai & Hutchison, 1989).

Once the reaction is completed, the gases are extracted, leaving the liquid silicon at the bottom of the furnace. The liquid silicon is collected in a melting pot, which feeds the casting where it solidifies. The temperature at which silicon is extracted from the furnace must be above that melting temperature of silicon (Enríquez-Berciano et al., 2009). However, if the temperature of silicon is too high, it can cause a premature wear of the refractory materials and increase the risk of dissolution of gases in the liquid silicon. On the contrary, low temperatures may result in low silicon fluidity (1573 K). While silicon stays in the melting pot, the refinement of silicon is carried out by an oxidative process, eliminating a large part of the impurities through the formation of slag. Silicon with a purity of 98%-99% is obtained through this process. In order to continuously feed the vessel of the continuous casting system, successive melting pots are operated in a sequential mode.

The melting pot discharges molten silicon into a distribution vessel. The vessel is opened when silicon can maintain a steady feeding flow. Silicon is then emptied into the ingot mold and cooled by water pipes located in the internal part reducing its temperature until it solidifies. Afterwards, solid silicon is cooled down using water showers to adjust its temperature to around 298 K before grinding in a roller crusher (Ceccaroli & Lohne, 2003). The Si_{MG} pieces obtained after grinding are stored at atmospheric conditions in a silo which feeds the chlorosilane synthesis reactor.

In the second stage, the grinded metallurgical grade silicon, hydrogen, and the $SiCl_4$ recycled from the next separation stage are fed in a fluidized bed reactor for chlorosilanes production. A rigorous model of $SiCl_4$-H_2-Si_{MG} system has been considered for this stage (Ding, et al., 2014). During this reaction, impurities such as Fe, Al, and B react to form their halides (e.g. $FeCl_3$, $AlCl_3$, and BCl_3). The $SiHCl_3$ has a low boiling point of 304.95 K and distillation is used to purify the $SiHCl_3$ from impurity halides. The purified $SiHCl_3$ contains less than 1 ppba of electrically active impurities such as Al, P, B, Fe, Cu or Au. According to Ding et al. (2014), it is assumed that the following species are involved in the $SiCl_4$-H_2-Si_{MG} system: $SiCl_4$, H_2, Si_{MG}, $SiHCl_3$, SiH_2C_{l2}, and HCl. A rigorous model of $SiCl_4$-H_2-Si_{MG} system has been developed for this stage, evaluating the effect of the operating conditions on the distribution of the products.

The reactor outlet stream contains a mixture of $SiCl_4$, $SiHCl_3$, SiH_2Cl_2, together with HCl and H_2. This stream is fed into a condensation stage that separates the reactor effluent in a gas phase stream and a liquid phase. The gas phase stream is formed by the most volatile compounds, H_2 and HCl, while the liquid stream is formed mainly by SiH_2Cl_2, $SiHCl_3$ and $SiCl_4$. Due to the large difference of volatility between the hydrogen, hydrogen chloride, and the chlorosilanes, a 100% separation efficiency in this stage is considered (Payo, 2008). Therefore, the gaseous stream in the condenser is cooled to 298 K. Here, the chlorosilanes condense until they reach a liquid phase. Afterwards, the stream is introduced into a phase separator where the gaseous hydrogen and hydrogen chloride are separated and stored in a tank, while the liquid stream consisting of the chlorosilanes is sent to the third stage.

The third step is a purification stage where two conventional distillation columns are used to separate the chlorosilanes mixture. The $SiCl_4$ is separated first, due to the large quantity that it represents. From the top of the first column a SiH_2Cl_2-$SiHCl_3$ mixture

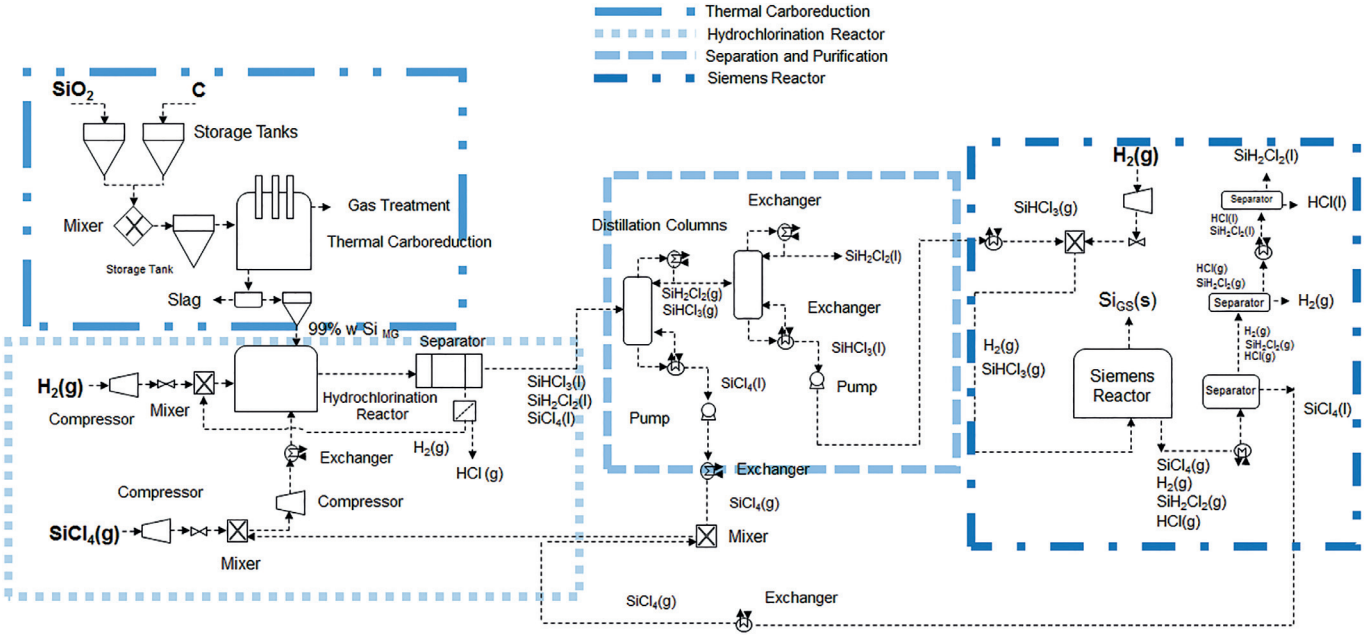

Fig. 4. Flowsheet of the Hybrid Process proposed.

is recovered, while from the lower section a high purity $SiCl_4$ is obtained. The second column separates the SiH_2Cl_2-$SiHCl_3$ mixture obtained from the dome of the previous distillation column, obtaining a high purity stream of SiH_2Cl_2 at the top, and a high purity stream of $SiHCl_3$ at the bottom (Ramírez-Márquez et al., 2018).

In the last stage $SiHCl_3$ is fed to the Siemens vapor deposition reactor. The Siemens reactor consists of a chamber where several thin high purity silicon rods are heated up by an electric current that flows through them. In the reactor, the thermal decomposition of trichlorosilane in a hydrogen atmosphere is carried out at temperatures of 373-873 K, leading to the silicon deposition on the rods, where the solar grade polysilicon is obtained. The reactor was modeled assuming a stoichiometric reactor (Ramírez-Márquez et al., 2018 and 2019). The optimization of reaction conditions, particularly gas flow and temperature, is pursued with the aim of finding an optimal trade-off between polycrystalline silicon growth and operation costs due to energy consumption.

The process diagram for polycrystalline silicon production that was used in this work is showed in Fig. 4. It shows all process sequence and the products generated in each stage.

3. Modeling approach

In this section, the description of the development of surrogate models for the three main reactors and the two distillation columns is presented. The other units of the process, i.e. compressors, heat exchangers, mixers and splitters are modeled based on first principles and thermodynamics (Martín, 2016). Note that the modeling approach to each unit is highly dependent on the type of experimental studies available in the literature and that its main limitation is in the use of any modeling technique. Regarding accuracy, each model was validated versus original data in order to reproduce the data within the same operating conditions.

3.1. Thermal carboreduction

The process starts with the carboreduction stage. The raw materials used are quartz (SiO_2) and carbon (C). These materials are stored in storage tanks, to be further blended in a mixer before being fed into the carboreduction reactor. The storage tanks and mixers have been modeled through material balances, being sized for purposes of cost estimation (Martín, 2016).

The model for the carboreduction reactor is based on the work reported by Wai and Hutchison (1989). Their work showed that the reaction among SiO_2 and C, Eq. (1), actually consists of a number of stages.

$$SiO_{2\,(S)} + 2C_{(s)}\Delta \rightarrow Si_{(l)} + 2CO_{(g)} \quad (1)$$

The detailed model proposed by Wai and Hutchison (1989) considers the multiple silicon dioxide reactions with carbon at high temperatures to form several products. The possible reactions that may take place during the silicon dioxide carboreduction process are shown in Eqs. (2) to (8).

$$SiO_{2\,(l)} + C_{(s)} \rightarrow SiO_{(g)} + CO_{(g)} \quad (2)$$

$$SiO_{2\,(l)} + C_{(s)} \rightarrow Si_{(l)} + CO_{2\,(g)} \quad (3)$$

$$SiO_{2\,(l)} + 2C_{(s)} \rightarrow Si_{(g)} + 2CO_{(g)} \quad (4)$$

$$SiO_{2\,(l)} + 2C_{(s)} \rightarrow Si_{(l)} + 2CO_{(g)} \quad (5)$$

$$SiO_{2\,(l)} + 2.5C_{(s)} \rightarrow 0.5Si_2C_{(g)} + 2CO_{(g)} \quad (6)$$

$$SiO_{2\,(l)} + 3C_{(s)} \rightarrow SiC_{(s)} + 2CO_{(g)} \quad (7)$$

$$SiO_{2\,(l)} + 4C_{(s)} \rightarrow SiC_{2\,(l)} + 2CO_{(g)} \quad (8)$$

Wai and Hutchison (1989) computed the products distribution for a C/SiO_2 feeding molar ratio of 2:1, a total pressure of 1 atm, and a temperature range of 2500-3500 K. To achieve the production capacity of typical industrial plants, in this work a feed of 15 kmol/h of SiO_2 and 30 kmol/h of C is considered. To model the carboreduction process, the distribution diagram of gaseous

and condensed species in the system Si-O-C at different temperatures obtained by Wai and Hutchison (1989) is used. Based on their work, correlations are developed to estimate the distribution of the products obtained at the reactor (mol fraction) as a function of the reaction temperature (K), considering a temperature range from 2600 to 3100 K.

The PlotDigitizer software was used for data extraction from plots. Thus, the fit of numerical data obtained for each one of the species was carried out as a function of the temperature, obtaining the following correlations for the distribution of the carboreduction products, Eqs. (9) to (16), where, x_i is the molar fraction of each species i, and T [K] is the temperature between the range of 2600 a 3100 K . Note that not all the correlations show the same mathematical shape. This is due to the complex shape of the distribution profiles.

$$x_{Si(l)} = -2.48131 \times 10^{-9}\ T^3 + 1.90239 \times 10^{-5}\ T^2 - 4.79395 \times 10^{-2}\ T + 39.71359 \quad (9)$$

$$x_{CO(g)} = 9.82689 \times 10^{-5}\ T^3 + 1.90239 \times 10^{-5}\ T + 3.74066 \times 10^{-1} \quad (10)$$

$$x_{Si(g)} = 5.93093 \times 10^{-10} e^{6.31510 \times 10^{-3} T} \quad (11)$$

$$x_{SiC(s)} = 7.14539 \times 10^{-7}\ T^2 - 4.50044 \times 10^{-3}\ T + 7.08465 \quad (12)$$

$$x_{Si2C(g)} = 1.72881 \times 10^{-7} T^2 - 9.13915 \times 10^{-4}\ T + 1.20759 \quad (13)$$

$$x_{SiC2(g)} = -1.19611 \times 10^{-14} T^5 + 1.65491 \times 10^{-10} T^4 - 9.14807 \times 10^{-7}\ T^3 + 2.52572 \times 10^{-3} T^2 - 3.48320\ T + 1919.64937 \quad (14)$$

$$x_{SiO(g)} = 7.58739 \times 10^{-7}\ T^2 - 4.47932 \times 10^{-3}\ T + 6.69671 \quad (15)$$

$$x_{Si2(g)} = 1 - x_{Si(l)} - x_{CO(g)} - x_{Si(g)} - x_{SiC(s)} - x_{Si2C(g)} - x_{SiC2(g)} - x_{SiO(g)} \quad (16)$$

The validation of the model can be viewed in the Supplementary material where the experimental data is plotted versus the model. Likewise, the energy balance to the reactor is performed to calculate the utilities required. To provide the necessary energy for the reaction electrodes are used. A power consumption of 10-11 kWh is required to produce a kilogram of silicon, reaching temperatures over 2600 K (Brage, 2003).

Regarding the post processing of the liquid product obtained, mainly melted silicon, the modeling of the discharge to the melting pot, the distribution pipe, the secondary cooling, and the roller crusher was carried out by material and energy balances. The second exit stream consisting of the gaseous components is sent to gas treatment. The solid SiC is extracted in the melting pot as slag, whereas the metallurgical silicon is sent to the solidification stage by cooling for its subsequent use in the chlorosilane synthesis reactor.

3.2. Hydrochlorination reactor

In the hydrochlorination reactor, the recycled $SiCl_4$ is hydrogenated in the presence of Si_{MG}. The thermodynamic analysis of the system $SiCl_4$–H_2–Si_{MG} performed from both thermodynamic and experimental perspectives by Ding et al. (2014) is considered to model this unit, where chlorosilanes are produced as intermediate products. The reactions of the $SiCl_4$–H_2–Si_{MG} system includes the $SiCl_4$ hydrogenation in gas phase, Eq. (17), and the hydrochlorination of Si_{MG} with HCl, Eq. (18).

$$SiCl_{4(g)} + H_{2(g)} \leftrightarrow SiHCl_{3(g)} + HCl_g \quad (17)$$

$$HCl_{(g)} + \frac{1}{3} Si_{MG(s)} \rightarrow \frac{1}{3} SiHCl_{3(g)} + \frac{1}{3} H_{2(g)} \quad (18)$$

Combining (17) and (18) yields the $SiCl_4$–H_2–Si_{MG} process, Eq. (19).

$$SiCl_{4(g)} + \frac{2}{3} H_{2(s)} + \frac{1}{3} Si_{MG(s)} \leftrightarrow \frac{4}{3} SiHCl_{3(g)} \quad (19)$$

The total Gibbs free energy minimization model, given by Eq. (20), is used to determine the products distribution at equilibrium.

$$G^T = \sum_{i=1}^{N} n_i \mu_i = \sum_{i=1}^{N} n_i \left(G_i^o + RT ln \frac{\widehat{f}_i}{f_i^o} \right) \quad (20)$$

Furthermore, considering the constraint defined by Eq. (21):

$$\sum_i n_i a_{ik} = A_K \ \ (k = 1,\ 2,\ \ldots,\ w) \quad (21)$$

The following equations are indicated for the gas-phase, defining the fugacity $\widehat{f}_i$, standard fufacity f_i^o, and molar fraction, y_i, given by Eqs. (22), (23) and (24), respectively.

$$\widehat{f}_i = y_i \widehat{\varphi}_i P,\ \ f_i^o = P^o,\ \ \ y_i = \frac{n_i}{\sum_i^N n_i} \quad (22)$$

For solid silicon:

$$RT ln \frac{\widehat{f}_i}{f_i^o} = \int_{P_o}^{P} V_{SiMG} (P - P^o) dP \quad (23)$$

since V_{SiMG} is almost independent of the pressure, it can be approximated by Eq. (24):

$$RT ln \frac{\widehat{f}_i}{f_i^o} = V_{SiMG} (P - P^o) \quad (24)$$

Therefore, combining Eqs. (20) to (24), Eq. (25) is obtained to describe the total Gibbs free energy of the system:

$$G^T = \sum_{i=1}^{N} n_i \left(G_i^o + RT ln \frac{y_i P}{P^o} \right) + n_{Si} G_{Si}^o + V_{SiMG} (P - P^o) \quad (25)$$

Where the Gibbs–Helmholtz relationship is defined by Eq. (26):

$$G_i^o = H_i^o + T S_i^o \quad (26)$$

The standard enthalpy and standard entropy are defined by Eqs. (27) and (28) respectively,

$$H_i^o = H_{i,298}^o + \int_{298}^{T} C_{p,i}\ dt \quad (27)$$

$$S_i^o = S_{i,298}^o + \int_{298}^{T} \frac{C_{p,i}}{T}\ dt \quad (28)$$

In these expressions, G^T is the total Gibbs free energy; N is the number of species in the reaction system; n_i is the number of moles; μ_i is the chemical potential; G_i^o is the standard Gibbs free energy; $\widehat{f}_i$ is the fugacity and f_i^o is the standard fugacity of species i; R is the molar gas constant; T is the temperature; a_{ik} is the number of k_{th} atoms in each molecule of species i; A_K is the total atomic mass of the k_{th} element in the system; w is the

total number of elements in the system; P is the total pressure. $\widehat{\varphi}_i$ is the fugacity coefficient; y_i is the molar fraction of species i; P^o is the standard-state pressure (100 kPa); V_{SiMG} is the molar volume of silicon; and H_i^o, S_i^o, and $C_{p,i}$ are the standard enthalpy, standard entropy, and heat capacity, respectively, of species i. Thermodynamic data for the chemical species involved is taken from Ding et al. (2014).

Using the model given by the Gibbs free energy minimization, it is possible to determine the species distribution when the reaction system reaches the equilibrium at different conditions of temperature, pressure and $H_2/SiCl_4$ molar feeding ratio. For convenience, the reaction system $SiCl_4-H_2-Si_{MG}$ was treated as ideal, and the following variables ranges were studied: temperature, 373–873 K; pressure , 1–20 atm; and molar feeding ratio $H_2/SiCl_4$, 1-5. The total Gibbs free energy minimization was performed offline using GAMS. A multi-start optimization approach using several nonlinear local solvers it was performed. This procedure was compared with solving the problem using Baron as solver and the same results were found. This model was used to develop surrogate models to be incorporated into the flowsheet optimization framework. The surrogates are developed for each one of the species involved in the reactions as shown in Eqs. (17) and (18) as a function of the three variables, temperature, pressure and $H_2/SiCl_4$ ratio are shown in Eqs. (29)-(33), where x_i is the equilibrium amount of the species i (mol fraction); P is the pressure (atm); T is the temperature (K); and Rel is the $H_2/SiCl_4$ molar feed ratio. The validation of the surrogate model obtained can be seen in the Supplementary material (section S.M.2).

$$x_{SiCl4(g)} = 5.345\times10^{-1} - 4.0\times10^{-6}\,P - 1.6805\times10^{-1}Rel + 1.7367\times10^{-2}\,Rel^2 + 1.0\times10^{-6}\,P*Rel \quad (29)$$

$$x_{SiHCl3(g)} = 2.3454\times10^{-1} + 4.0\times10^{-6}\,P - 7.369\times10^{-2}\,Rel - 8.0\times10^{-6}\,T + 7.633\times10^{-3}\,Rel^2 + 1.0\times10^{-6}\,T\,Rel*T \quad (30)$$

$$x_{SiH2Cl2(g)} = 2.781\times10^{-2} + 1.0\times10^{-6}\,P - 9.358\times10^{-3}\,Rel + 4\,.0\times10^{-6}T + 1.031\times10^{-3}\,Rel^2 \quad (31)$$

$$x_{H2(g)} = 2.048\times10^{-1} - 6.0\times10^{-6}\,P + 2.505\times10^{-1}\,Rel + 2.0\times10^{-6}\,T - 2.6166\times10^{-2}Rel^2 + 1.0\times10^{-6}\,P*Rel \quad (32)$$

$$x_{HCl(g)} = 1 - x_{SiCl4(g)} - x_{SiHCl3(g)} - x_{SiH2Cl2(g)} - x_{H2(g)} \quad (33)$$

The condensation step was modeled based on material and energy balances considering complete separation of the effluent in a gas phase stream and a liquid phase stream. The phase separator in which the hydrogen and hydrogen chloride gaseous are separated from the liquid chlorosilanes stream was modeled through material balances and their respective energy balance assuming perfect separation based on experimental results (Payo, 2008).

3.3. Separation and purification

For the separation of the chlorosilanes two conventional distillation columns are used. The rigorous modeling and sizing of the columns was performed using the Aspen Plus® software based on previous work (Ramírez-Márquez et al., 2019). The Aspen Plus® models of the distillation columns were used to obtain surrogate models for optimization. A number of runs were performed under different conditions for key variables such as reflux ratio and feed composition obtaining as response the energy involved in the reboiler and at the condenser, and the operating temperatures. The product purity, the diameter and the height of the distillation columns are fixed in the simulations while the effect of the feed and the reflux ratios on the energy and operating temperatures of each column were evaluated. The variables were evaluated in the following ranges: feeding molar ratio $SiCl_4$-(SiH_2Cl_2-$SiHCl_3$) values from 1 to 2.1698 for the first column; SiH_2Cl_2 - $SiHCl_3$ feed molar ratio from 2.99 to 7.5678 for the second column; and reflux ratio from 10 to 80 for the first column and from 60 to 90 for the second column. The limits of the input variables of the distillation column were based on mechanical considerations (Górak and Olujic, 2014) and were analyzed based on a feasibility analysis carried out in Aspen Plus®. Surrogate models were developed from the data obtained in the simulations. Eqs. (34) to (41) show the computed variables including the reboiler and condenser thermal duties, as well as the top and bottom temperatures.

$$Q_{ConCol1} = -497.162 + 150.215\,FR - 495.071\,RR - 2.17\times10^{-4}\,RR^2 + 150.191\,FR*RR \quad (34)$$

$$Q_{RebCol1} = 909.868 - 209.970\,FR + 495.071\,RR + 2.14\times10^{-4}\,RR^2 - 150.191\,FR*RR \quad (35)$$

$$T_{ConCol1} = 351.296 - 4.93\times10^{-4}\,RR - 1.70050\,FR + 6\times10^{-6}RR^2 - 1.0\times10^{-4}\,RR*FR \quad (36)$$

$$T_{RebCol1} = 387.695 - 9.0\times10^{-6}\,FR \quad (37)$$

$$Q_{ConCol2} = -15.777 - 1.1074\,FR - 18.3726\,RR + 1.0438\times10^{-1}\,FR^2 + 1.0\times10^{-6}\,RR^2 + 3.632\times10^{-3}\,FR*RR \quad (38)$$

$$Q_{RebCol2} = 19.968 + 9.4538\,FR + 18.3726\,RR - 1.0427\times10^{-1}\,FR^2 - 1.0\times10^{-6}\,RR^2 - 3.632\times10^{-3}\,FR*RR \quad (39)$$

$$T_{ConCol2} = 321.8 - 1\times10^{-6}\,FR \quad (40)$$

$$T_{RebCol2} = 346.2 + 1.714\,FR - 1.057\times10^{-1}\,FR^2 \quad (41)$$

where, $Q_{ConCol1}$ is the condenser heat duty of the column 1 (kW); $Q_{RebCol1}$ is the reboiler heat duty of the column 1 (kW);$T_{ConCol1}$ is the top temperature of the column 1 (K);$T_{RebCol1}$ is the bottom temperature of the column 1 (K); $Q_{ConCol2}$ is the condenser heat duty of the column 2 (kW); $Q_{RebCol2}$ is the reboiler heat duty of the column 2 (kW);$T_{ConCol2}$ is the top temperature of the column 2 (K);$T_{RebCol2}$ is the bottom temperature of the column 2 (K); FR is the Feed Ratio; RR is the Reflux Ratio.

The mass balances were considered as follows: in the first column dome a SiH_2Cl_2-$SiHCl_3$ mixture is recovered, whose composition depends on the operating conditions of the hydrochlorination reactor, while in the bottom of the column high purity $SiCl_4$ (99.999% wt.) is obtained. The second distillation column separates the SiH_2Cl_2-$SiHCl_3$ mixture, obtaining high purity SiH_2Cl_2 in the dome (99.999% wt.), while for the lower section a high purity $SiHCl_3$ (99.999% wt.) is recovered (Ramírez-Márquez et al., 2018).

The surrogate model validation can be seen in the Supplementary material (section S.M.3).

3.4. Siemens reactor

The deposition of polycrystalline silicon was modeled according to the work by Del Coso et al., 2008. In their work, the operating conditions required for polycrystalline silicon deposition in the traditional Siemens reactor are provided. They develop analytic solutions for the deposition process, splitting the second-order reaction rate into two systems of first-order reaction rate. The growth rate, the deposition efficiency, the power-loss dependence on the gas velocity, the composition of the mixture of gas, the reactor pressure, and the surface temperature have been analyzed, providing information regarding the deposition velocity and the polycrystalline silicon quantity obtained. The variables analyzed were the polysilicon growth rate, the deposition efficiency and the system temperature. The U shape bars of ultrapure silicon of the Siemens reactors are heated up using electric current. The variables described above are studied in the reaction system formed by the reactions showed in Eqs. (42) and (43) (Del Coso et al., 2008; Jain et al., 2011).

$$SiHCl_3 + H_2 \leftrightarrow Si + 3\ HCl \tag{42}$$

$$SiHCl_3 + HCl \leftrightarrow SiCl_4 + H_2 \tag{43}$$

It is assumed that silicon deposition follows a second order kinetics, where the consumption or generation mass rate of the species i in the surface of the rods can be expressed as Eq. (44):

$$R_i = \nu_i \mu_i k [SiHCl_3][H_2] \tag{44}$$

where, R_i is the mass rate of species i by chemical reaction, [kg/m^{2}s]; μ_i is the viscosity of the species i, [kg /m s]; ν_i corresponds to the stoichiometry coefficients of the compounds involved in the reactions (−1 for $SiHCl_3$ and H_2 and 3 for HCl); k is the overall reaction coefficient; and [i] is the mole concentration of species $i$on the surface.

The global deposition reaction coefficient can be expressed as shown in Eq. 45, where, k_{ad} is the rate of $SiHCl_3$ chemisorption on the surface; and k_r is the trichlorosilane decomposition rate.

$$\frac{1}{k} = \frac{[SiHCl_3]}{k_r} + \frac{[H_2]}{k_{ad}} \tag{45}$$

The kinetic coefficients are temperature dependent. Therefore, the Arrhenius's law applied at atmospheric pressure is considered, as shown in Eqs. (46) and (47), where, T is the temperature (K); and R is the constant of ideal gases in SI units.

$$k_{ad}(T) = 2.72 \times 10^6 exp\left(\frac{-1.72 \times 10^5}{RT}\right) \tag{46}$$

$$k_r(T) = 5.63 \times 10^3 exp\left(\frac{-1.80 \times 10^5}{RT}\right) \tag{47}$$

The model defined by Eqs. (44)-(47) was solved with the data reported by Del Coso et al., 2008 for a temperature range from 1372 to 1500 K. As in the previous cases, a surrogate model is developed to estimate the species distribution as a function of the temperature in the range studied, Eqs. (48)-(51). It should be noted that the reaction coefficients estimated through Eqs. (46) and (47) are validated at atmospheric pressure, and consequently, they should not be used to calculate the effect of pressure inside the reactor.

$$X_{Si(s)} = -6.220 \times 10^{-7} T^2 + 1.8580059 \times 10^{-3} T - 1.3159371763 \tag{48}$$

$$X_{H2(g)} = 3.9 \times 10^{-9} T^2 - 1.17934 \times 10^{-5} T + 1.47006954 \times 10^{-2} \tag{49}$$

$$X_{HCl(g)} = 3.57 \times 10^{-8}\ T^2 - 1.066805 \times 10^{-4}\ T + 1.329638743 \times 10^{-1} \tag{50}$$

$$X_{SiCl4(g)} = 1 - X_{Si(s)} - X_{H2(g)} - X_{HCl(g)} \tag{51}$$

where, X_i is the concentration of the species i (mass fraction) and T is the temperature (K). The polycrystalline silicon deposition itself, is the largest contributor to the energy consumption of the overall process is assumed to be 60 kWh per kg (Ramos et al., 2015). The validation of the surrogate model obtained for polycrystalline silicon deposition can be found in the Supplementary material (section S.M.4). It can be noticed that the approximation of the models is quite precise to those obtained by Del Coso et al., 2008.

The silicon rods grow continuously to a thickness of 80 mm–150 mm per rod (Ramos et al., 2015). Electrical power is used to heat the rods. The deposition process takes about 3 to 5 days (Ramos et al., 2015). Therefore, it is necessary to use several deposition reactors for the required production.

3.5. Auxiliary equipment

Pumps, separators and heat exchangers were modeled according to mass and energy balances in steady state. Regarding compressor modeling, polytrophic behavior for all compressors was considered, as well as an efficiency, n_c, of 0.85 (Walas, 1990), the polytrophic coefficient, z, was obtained from Aspen Plus® offline simulations, having a value of 1.4. Energy balance for compressors was estimated considering Eqs. (52) and (53).

$$T_{outCompressor} = T_{inCompressor} + T_{inCompressor}\left(\left(\frac{P_{outCompressor}}{P_{inCompressor}}\right)^{\frac{z-1}{z}} - 1\right)\frac{1}{n_c} \tag{52}$$

$$W_{(Compressor)} = F \cdot \left(\frac{R \cdot z \cdot \left(T_{inCompressor}\right)}{((M_w) \cdot (z-1))}\right) \cdot \frac{1}{n_c} \cdot \left(\left(\frac{P_{outCompressor}}{P_{inCompressor}}\right)^{\frac{z-1}{z}} - 1\right) \tag{53}$$

where, $T_{outCompressor}$ is the outlet temperature (K); $T_{inCompressor}$ is the inlet temperature (K); $P_{outCompressor}$ is the outlet pressure (kPa); $P_{inCompressor}$ is the inlet pressure (kPa); z is a polytrophic coefficient; n_c is the efficiency of the compressor; $W_{(Compressor)}$ is the electrical energy (kW); and R is the constant of ideal gases in SI units.

4. Solution procedure

The process was formulated as a nonlinear programming (NLP) problem. The model consists of 1,281 equations and 1,695 variables. Three different objective functions, Eqs. (54) to (56), are evaluated for the optimization of the Hybrid Process for polycrystalline silicon production considering the following decision variables: the temperature of the thermal carboreduction reactor; the temperature, pressure, and $H_2/SiCl_4$ feeding molar ratio of the hydrochlorination reactor, the feeding ratio and the reflux ratio of each distillation column, and the operating temperature of the Siemens Reactor, see Table 1.

Table 1
Summary of decision variables for the process.

	TCarb			Hydro			Separation		Siemens
					Column 1		Column 2		
Variables	T[K]	T[K]	P [kPa]	$H_2/SiCl_4$	FR	RR	FR	RR	T [K]

TCarb=Thermal Carboreduction; Hydro=Hydrochlorination Reactor; T= Temperature; P=Pressure; FR= Feed Ratio; RR= Reflux Ratio.

Table 2
Operating conditions of each stage of the process.

	TCarb			Hydro			Separation		Siemens
					Column 1		Column 2		
OF	T[K]	T[K]	P [kPa]	$H_2/SiCl_4$	FR	RR	FR	RR	T [K]
1	2859.65	673.15	2026.00	1.92	2.17	80.00	6.82	90.01	1493.57
2	2776.91	873.25	2026.00	5.00	2.09	13.89	5.06	59.99	1372.50
3	2868.71	873.25	2026.00	4.56	2.09	13.92	5.15	59.99	1500.50

* OF= Objective function; TCarb=Thermal Carboreduction; Hydro=Hydrochlorination Reactor; T= Temperature; P=Pressure; FR= Feed Ratio; RR= Reflux Ratio.

The first objective function, Eq. (54), seeks to maximize the polycrystalline silicon production where, $fc_{polycrystalline\,silicon}$ is the mass flow of polycrystalline silicon.

$$\textbf{OF1})\ z = fc_{polycrystalline\ silicon} \tag{54}$$

The second objective function, Eq. (55), aims to minimize the process operation cost according to the methodology demonstrated by Gutiérrez (2003), where, a is a factor that considers annual expenses such as maintenance; I_F is the fixed annualized investment; b is the unit cost of each raw material RM; c is the cost of each utility E; $d\,MO$ is the cost of manpower; p is the price of each by-product SP. The raw material, vapor, cooling and electricity costs are taken from the report of Intratec Solutions (2019).

$$\textbf{OF2})\ min\ z = a\ I_F + b\ RM + c\ E + d\ MO - p\ SP \tag{55}$$

Finally, the third objective function, Eq. (56), aims to maximize the process total profit, considering not only the production of the main product (polysilicon), but also the income from byproducts (chlorosilanes), deducting the manufacturing cost, where, $S_{polycrystalline\,silico}$ is profit from the sale of the polycrystalline silicon.

$$\textbf{OF3})z = S_{polycrystalline\ silico} + p\ SP - b\ RM - c\ E \tag{56}$$

Each one of the problems are formulated as an NLP solved using a multistart initialization approach with CONOPT as the preferred solver.

Also, a detailed economic evaluation based on Turton et al. (2012) procedure is carried out for the facility proposed, estimating the equipment cost, production cost, maintenance, administration and manpower.

5. Results

5.1. Operating conditions

The optimization of the polycrystalline silicon production plant is evaluated under three different optimization criteria as described in the section "Solution procedure". The values of the decision variables for the process optimization, and the energy requirements and temperatures using the different objective functions are shown in Tables 2 and 3 respectively.

The first objective function, OF 1, maximizes the polycrystalline silicon production. The results obtained show two features. First, for a large production of silicon, the hydrochlorination reactor temperature is low using a $H_2/SiCl_4$ molar ratio of 1.92. However, despite the low energy requirement of the reactor, the production costs of $SiHCl_3$ are high due to the use of considerable amounts of $SiCl_4$. The second particularity is that the process requires high energy consumption in the distillation columns due to the high values of the reflux ratios, ensuring a high polycrystalline silicon production capacity, although the operating cost is also high.

Regarding the second objective function, the one that minimizes of the operating cost, the carboreduction reactor shows a lower operating temperature, involving a moderate metallurgical silicon production rate. However, this guarantees lower energy consumption, as observed in Table 3. In the hydrochlorination reactor, the operating temperature of 873.25 K and the $H_2/SiCl_4$ feeding ratio of 5, guarantee a high $SiHCl_3$ production. Finally, the distillation columns and the Siemens reactor exhibit a low thermal load. This results in a process with a minimum operation cost, although, it is translated in a lower polycrystalline silicon production.

Finally, the third scenario corresponds to the profit maximization. In this scenario the reflux ratios are similar to the case of optimizing OF2 but the feed ratio to the hydrogenation reactor decreases to 4.56. The temperature of the Siemens reactor is slightly higher than in the previous cases. All scenarios consider the production of the required amount of polycrystalline silicon, as well as the high added value by-products which improves the profitability of the process.

The operating conditions of the process proposed are compared with the operating conditions of the existing industrial silicon polycrystalline to give a real picture of the optimized process.

In the first part of the process, thermal carboreduction of quartz, a large amount of energy is required to melt the quartz and take it to Si_{MG}. Brage (2003) reports industrial operating conditions for this stage of 2600 K at atmospheric pressure. The temperatures obtained for all scenarios, between 2700-2900 K at atmospheric pressure, are accordingly to the data reported by Brage (2003). The variation of temperature in the furnace depends on whether the target is a larger production of polycrystalline silicon, to reduce operating costs or to raise the profits of the process.

Erickson and Wagner (1952) reported experimental data for the $SiHCl_3$ production in a fluidized bed reactor. Typical operating conditions of 500-900 K and 2000-3600 kPa are required to obtain higher conversion. The results obtained ranging from 673 to 873 K and 2026 kPa (see Table 2) are according to these values. Once the $SiHCl_3$ is obtained, it is purified on a set of distillation columns. These columns operate in the range obtained by the rigorous simulation performed in Aspen Plus. These conditions are collected in Table 2.

Table 3
Energy requirements and temperatures for each objective function.

	TCarb	Hydro	Separation		Siemens		Comp		Exchanger	
	Column 1				Column 2				St	Co
OF	Q [kW]	Q [kW]	Q_{Con}/Q_{Reb} [kW]	T_{Con}/T_{Reb} [K]	Q_{Con}/Q_{Reb} [kW]	T_{Con}/T_{Reb} [K]	Q [kW]	W [kW]	Q [kW]	
1	4308.24	568.809	-13710/ 13989	347.60/ 387.695	-1669.95/ 1731.09	321.80/ 352.97	14,560.00	334.34	1040.36	-3242.90
2	4028.80	2140.52	-2700.00/ 2987.78	347.73/ 387.69	-1119.77/ 1166.26	321.80/ 352.17	11,571.86	708.83	1086.77	-6623.58
3	4345.68	2363.79	-2700.00/ 2987.65	347.73/ 387.69	-1119.75 /1166.96	321.80/ 352.22	15,755.12	781.54	1183.3	-7123.78

*Comp=Compressors; Exch= Exchanger; St= Steam; Co=Coolant; Q= Heat Duty; Con=Condenser; Reb=Reboiler; W=Work.

Table 4
Profit [M$/y], Operating costs [M$/y], and kg of polycrystalline silicon/h of each objective function.

OF	1	2	3
Profit [M$/y]	6.34	9.09	10.1
Operating costs [M$/y]	11.64	6.32	6.48
kg of polycrystalline silicon/h	236.71	173.641	217.752

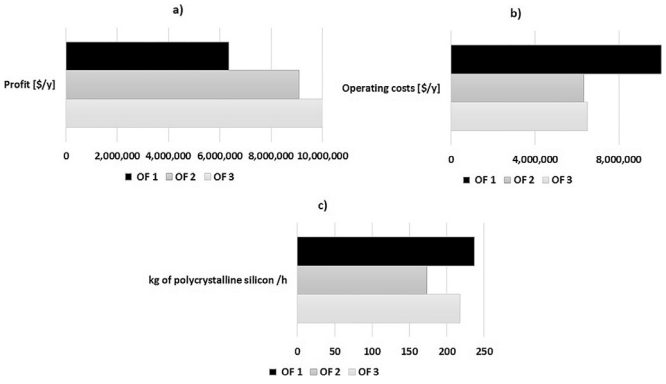

Fig. 5. a) Profit, b) Operating cost, c) kg of polycrystalline silicon/h of each objective function.

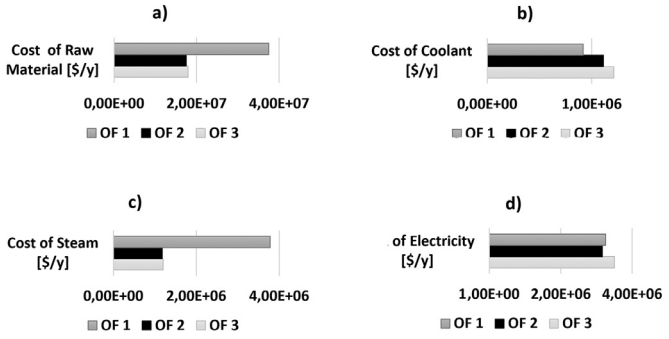

Fig. 6. Utility and raw material costs of each objective function.

Siemens reactor conditions are a temperature range between 1300 K and 1500 K and pressure is around 100 kPa according to Pazzaglia et al. (2011). These results are very similar to those obtained in the optimization, which range between 1370-1500 K at 100 kPa, as shown in Table 2. For the capacity of 2000 ton/y of polycrystalline silicon, 25 Siemens reactor units are required to complete the production.

5.2. Economic evaluation

The results shown in Table 4 summarize the economic parameters of the process. The larger the polycrystalline silicon production obtained optimizing the process proposed using OF1 does not result in a larger profit. The adequate arrangement of the operation conditions of each unit, the by-products generation, the raw material consumption, and the services consumption, are the ones that give a maximum profit in the process of 10 M$/y, see Fig. 5. This is an interesting result, and may lead to the development of a silicon multiproduct refinery rather than the production of Si_{SG} alone. Fig. 6 shows the consumption of each one of the utilities and raw materials for each one of the objective functions evaluated, showing that the maximum polycrystalline silicon production is associated with high costs in raw material.

Table 4 shows the optimal solutions for the three objective functions. If OF1 is considered, the production of polycrystalline silicon is maximized, producing 63.07 kg/h of polycrystalline silicon more than in case of using OF2, and 18.96 kg/h of polycrystalline silicon more than that of OF3. In the OF1 scenario, the increase of polysilicon production is not associated with a decrease in the production cost since the polysilicon production is maximized independently use of raw materials and utilities. On the other hand, the production of some secondary components such as $SiCl_4$, H_2, HCl is reduced, which can be sold to increase the profit of the process.

In the case of OF2, the production of polycrystalline silicon is drastically reduced, since the aim is to minimize the operation costs of the process, adjusting the production of silicon to the economy of the facility to reach the lower production cost feasible. By reducing the operating costs of the process, 5.32 M$/y with respect to OF1 and 0.16 M$/y with respect to OF3, the profit of the process increases as it has lower expenditure on raw materials and energy requirements. Like the previous case, all operating conditions, the required raw materials, and the economic performance of the facility are linked.

For OF3, where the profit of the facility is maximized, a larger amount of polysilicon compared to the OF2 scenario is produced. Operating costs are reduced to a value very similar to that of the previous scenario.In terms of the operation of the process, the production of secondary products which raise the profit of the process is promoted to improve the profit of the process. Additionally, the lowest production price of polycrystalline silicon 8.93 $/kg is obtained, below than the commercial price of 10 $/kg (PVinsights, 2019) and making the Hybrid Process a profitable and competitive process in the PV industry.

The equipment cost of the polycrystalline silicon plant results in $9.97 M. The investment cost is disaggregated in Table 5. The distillation columns are the most expensive, second by the Siemens reactor and the thermal carboreduction reactor. This equipment represents 77% of the total cost of the process.

To assess the benefits of the modelling approach developed in this work, the results of this work are compared with those of the process developed in Aspen Plus® by Ramírez-Márquez et al. (2019), see Table 6. It should be noted that in this work rigorous Aspen Plus® simulations are used to develop the surrogate models for the distillation columns, which are embedded in the optimization problem. It can be observed that in the previous optimization performed in Aspen Plus® the energy required by each stage, and therefore, the operation costs, are larger than

Table 5
Costs per equipment.

Equipment	Number of units	Total Cost ($USD)	Total Annualized Cost ($USD/y)
Tanks	4	$49,120.99	$9,824.20
Mixers	3	$262,601.81	$52,520.36
Thermal Carboreduction Reactor	1	$1,488,607.01	$297,721.40
Melting pot	1	$78,798.85	$15,759.77
Conveyor belt	1	$358,000.00	$71,600.00
Hydrochlorination Reactor	1	$265,252.64	$53,050.53
Chlorosilanes separator	1	$238,587.79	$47,717.56
Compressors	4	$928,308.52	$185,661.70
Heat exchanger	4	$112,678.95	$22,535.79
Distillation Columns	2	$3,915,626.17	$783,125.23
Siemens Reactor	25	$2,272,813.21	$454,562.64
Total	$9,970,395.94	$1,994,079.18	

* 5 years for the annualization.

Table 6
Comparison of operating conditions.

	TCarb			Hydro				Siemens			Si_{Poly}
	T[K]	P [kPa]	Q [kW]	T[K]	P [kPa]	$H_2/SiCl_4$	Q [kW]	T [K]	P [kPa]	Q [kW]	[ton/y]
1	2,859.65	100	4,308.24	673.15	2,026.00	1.92	568.80	1,493.57	100	14,560.00	2,012.04
2	2,776.91	100	4,028.80	873.25	2,026.00	5.00	2,140.52	1,372.50	100	9,571.86	1,475.94
3	2,868.71	100	4,345.68	873.25	2,026.00	4.56	2,363.79	1,500.50	100	12,755.12	1,850.89
Aspen Simulation	2,273.00	100	6,798.00	773.00	3,600.00	0.01	2,551.96	1,373.00	100	1,871.93	1,899.07

* **Si_{Poly}=Polycrystalline silicon**

the energy requirements obtained in the facility design proposed in this work. The production capacity is only similar when the polysilicon production is maximized (OF1 scenario). In the other scenarios, the system adjusts the production capacity to reduce the manufacturing costs to reach an optimal production cost. It can therefore be observed how the proposed methodology, combining rigorous column modeling and detailed surrogate models for the reactors with the optimization of the entire plant, results in an optimized design of the process with improved performance.

5.3. Scale-up study

Polycrystalline silicon technology relies on processes that have been mainly borrowed from the semiconductor industry. Consequently, unitary equipment, machines and accessories essential for the industrial process are also widely available. In the past two decades, the manufacturing of equipment, machines and accessories has increased in capacity and efficiency (Ranjan et al., 2011). Due to the experience of maintenance and operation, heuristics for such equipment are extensive and easily manageable. Therefore, by employing processes for which the equipment and supporting infrastructure are predominant, researchers may be able to ensure a degree of scalability in their technologies. However, when transitioning to higher production volumes, it becomes a challenge to consistently produce large quantities of polycrystalline silicon with the same quality.

In this work, the reference capacity of the facility is chosen to be 2.000 t/y. Although a decrease in the price of silicon was observed, this capacity is not large enough to have low manufacturing costs derived from economies of scale. Nowadays, the accepted value for the minimum capacity of a polysilicon plant is around 15,000 t/y. For this reason, a scaling study was carried out with values of around 5,000, 10,000, 15,000 and 20,000 t/y of polycrystalline silicon. As the size of the polycrystalline silicon production plant increases, the cost of plant investment increases as well due to larger or additional equipment is required. The scale-up study was carried out using the same methodology described previously for the modelling of the process and to estimate the equipment and operating costs. Since the lowest polysilicon price is obtained

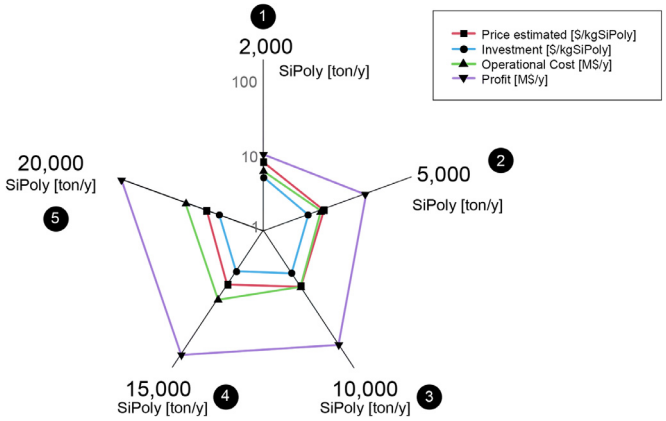

Fig. 7. Effects of scaling study for the Hybrid Process.

maximizing the profit of the facility, the objective function used in the scaling study is OF 3.

Table 7 shows the results of the scaling of the polycrystalline silicon plant. The increase in investment costs, production and profits along the capacity of the process is observed. A raise of the profit of 100% when the production capacity is increased from 2000 t/y to 20,000 t/y. Similarly, the price of polycrystalline silicon decreases 1.03$/kg$Si_{Poly}$ for the same capacity range.

Fig. 7 shows summarizes economic performance of polycrystalline silicon for the difference facility sizes evaluated collected in Table 7. In this figure, five axes that present the production capacity of the facility, and four items in each of the axes are addressed, such as the estimated price of polycrystalline silicon, the investment for each kilogram of silicon obtained, the operating costs and the profit of the facility. It can be observed a non-linear growth of each one of the items as a function of the capacity of the facility since.

Responsiveness of these scenarios proves an opportunity for both research and industry. By understanding the characteristics of production processes, equipment and the divergence from those used in a low scale, the process factors that drive them and the

Table 7
Results of scaling study for the Hybrid Process.

SiO_2 [kmol/h]-C [kmol/h]	Si_{Poly} [kg/h]	Si_{Poly} [t/y]	Price estimated [$/kg]	Investment [M$]	Operational Cost [M$/y]	Profit [M$/y]
15-30	217.752	1850.892	8.94	9.97	6.48	10.1
40-80	591.183	5025.0555	8.71	24.96	8.01	38.25
80-160	1168.78	9934.63	8.49	50.3	8.86	81.19
120-240	1825.284	15514.914	8.07	75.68	14.37	118.41
160-320	2369.137	20137.6645	7.91	99.16	15.98	157.11

changes upon scaling up can be anticipated. In fact, by studying the attributes, constraints, and practical limitations of large-scale processes, the conditions necessary to produce the desired product amount at scale can be learnt.

6. Conclusions

In this work the surrogate based optimization of a polycrystalline silicon production process based on the hybridization of the Siemens and the Union Carbide Co. processes developed in previous works (Ramírez-Márquez et al., 2018, 2019) is performed. Each unit has been modeled in detail. The entire process, and therefore the operating conditions of each unit of the process were optimized under three objective functions: the maximization of the production of polycrystalline silicon, the maximization profit of the process, and the minimization of operating costs. The advantage of evaluating the process under the three objective functions is to determine the effect of the operating conditions under each objective function showing that the maximum production of the target compound does not always guarantee a lower selling price. The optimal operating conditions of the facility that guarantee a lower energetic consumption, meeting with the required production of polycrystalline silicon require the production of high valuable byproducts which aid in the economic sustainability of the process. The results of each objective function show advantages and disadvantages. For a large production of polycrystalline silicon, operating costs increase. If the operating costs are minimized, the production of polycrystalline silicon is low. By maximizing the profit of the process, a trade-off between the last two objective functions is achieved. For this last scenario, the results after operating expenses, and considering the sale of polycrystalline silicon and the byproducts of the process, are an operational cost of 6.48 M$/y. The investment for the process is 9.97M$. Obtaining a competitive production cost for polycrystalline silicon of 8.93 $/kg, below the commercial price estimated at 10 $/kg. Also, a decrease in the price of polycrystalline silicon is observed if the production size of the polycrystalline silicon plant is increased, the price was reduced by 1.03 $/kg$Si_{Poly,}$ increasing production 10 times. Additionally, the advantages of optimizing the development of customize optimization methods, in contrast with the use of generic equipment models in the previous works developed in the Aspen Plus® software has been shown.

Declaration of Competing Interest

The authors declare that they have no known competing financial interests or personal relationships that could have appeared to influence the work reported in this paper.

Acknowledgements

The authors acknowledge CONACyT (Mexico), Universidad de Guanajuato and PSEM3 at Universidad de Salamanca.

Supplementary materials

Supplementary material associated with this article can be found, in the online version, at doi:10.1016/j.compchemeng.2020.106870.

Appendix A

Energy balances

The energy balance to an open system in steady state is described by the Eq. (57) (Doran, 2013).

$$\Delta E_C + \Delta E_P + \Delta H = Q + W \tag{57}$$

where, ΔE_C is the variation of kinetic energy; ΔE_P is the variation of potential energy; ΔH is the enthalpy variation; Q is the heat exchanged by the system; and W is the work exchanged by the system.

In this work, the mechanic energy contributions (kinetic and potential energy) to the system total energy were considered negligible compared with the other terms. Thus, the energy balance is simplify, obtaining the Eq. (58):

$$\Delta H = Q + W \tag{58}$$

The enthalpy variation respect to a reference state is defined according to the Eq. (59):

$$\Delta H = \sum_i n_i \cdot \int_{TRef}^{T} C_{pi} \cdot dt + \sum_i n_i \cdot \lambda_i + \sum_i n_i \cdot H_{fi}^{Tref} \tag{59}$$

where, n_i is the amount of the component i; T is the temperature [K];C_{pi} is the specific heat of the component i; λ_i is the specific latent heat for each element *i*; H_{fi}^{Tref} is the standard enthalpy for each element *i*.

The first term of Eq. (59) refers to the energy replaced due to a temperature change (called sensible heat), and it is represented as Q_S. The second term, called sensible heat, shows the heat involved if a phase change of the considered substance occurs, and it is represented as Q_L. Finally, the third term shows the energy associated with the substance formation through a chemical reaction (called reaction heat), and it is represented as QR. The thermodynamic data required in the modeling of the different processes was taken from the National Institute of Standards and Technology (2018).

References

Audet, C., Denni, J., Moore, D., Booker, A., Frank, P., 2000. A surrogate-model-based method for constrained optimization. In 8th Sympos. Multidiscip. Anal. Optim. 4891. doi:10.2514/6.2000-4891.

Brage, F.J.P., 2003. Contribución al modelado matemático de algunos problemas en la metalurgia del silicio (Doctoral dissertation. Universidad de de Santiago de Compostela).

Caballero, J.A., Grossmann, I.E., 2008. An algorithm for the use of surrogate models in modular flowsheet optimization. AIChE J. 54 (10), 2633–2650. doi:10.1002/aic.11579.

Ceccaroli, B., Lohne, O., 2003. Solar grade silicon feedstock. Handb. Photovolt. Sci. Eng. 153–204. doi:10.1002/0470014008.ch5.

Chigondo, F., 2018. From metallurgical-grade to solar-grade silicon: an overview. Silicon 10 (3), 789–798. doi:10.1007/s12633-016-9532-7.

Del Coso, G., Del Canizo, C., Luque, A., 2008. Chemical vapor deposition model of polysilicon in a trichlorosilane and hydrogen system. J. Electrochem. Soc. 155 (6), D485–D491. doi:10.1149/1.2902338.

Ding, W.J., Yan, J.M., Xiao, W.D., 2014. Hydrogenation of silicon tetrachloride in the presence of silicon: thermodynamic and experimental investigation. Indust. Eng. Chem. Res. 53 (27), 10943–10953. doi:10.1021/ie5019222.

Doran, P.M., 2013. Bioprocess engineering principles, Chapter 5 - Energy Balances. Elsevier 139–176. doi:10.1016/B978-0-12-220851-5.00005-8.

Erickson, C. E., &Wagner, G. H. (1952). U.S. Patent No. 2,595,620. Washington, DC: U.S. *Patent and Trademark Office*.

Enríquez-Berciano, J.L., Tremps-Guerra, E., Fernández-Segovia, D., de Elío de Bengy, S., 2009. Monografías sobre Tecnología del Acero. Parte III: Colada del acero. Universidad Politécnica de Madrid.

Fahmi, I., Cremaschi, S., 2012. Process synthesis of biodiesel production plant using artificial neural networks as the surrogate models. Comp. Chem. Eng. 46, 105–123. doi:10.1016/j.compchemeng.2012.06.006.

Górak, A., Olujic, Z. (Eds.), 2014. Distillation: equipment and processes. Academic Press.

Green, M.A., 2009. The path to 25% silicon solar cell efficiency: history of silicon cell evolution. Progr. Photovolt. Res. Appl. 17 (3), 183–189. doi:10.1002/pip.892.

Gutiérrez, A.J., 2003. Diseño de procesos en ingeniería química. Reverté 8–27.

Henao, C.A., Maravelias, C.T., 2010. Surrogate-based process synthesis. In: Computer Aided Chemical Engineering (Vol, 28. Elsevier, pp. 1129–1134. doi:10.1016/S1570-7946(10)28189-0.

Hesse, K., Schindlbeck, E., Dornberger, E., Fischer, M., 2009. Status and development of solar-grade silicon feedstock. In 24 thEuropean Photovolt. Solar Energy Conf. 883–885.

Intratec Solutions, 2019. Examine Production Costs of Chemicals. San Antonio. United States of America Publishing, TX. Recovered from https://www.intratec.us/ .

Iya, S.K., 1986. Production of ultra-high-purity polycrystalline silicon. J. Crystal Growth 75 (1), 88–90. doi:10.1016/0022-0248(86)90228-9.

Jain, M.P., Sathiyamoorthy, D., Rao, V.G., 2011. Studies on hydrochlorination of silicon in a fixed bed reactor. Indian Chem. Eng. 53 (2), 61–67. doi:10.1080/00194506.2011.659537.

Kato, K., Wen, C.Y., 1969. Bubble assemblage model for fluidized bed catalytic reactors. Chem. Eng. Sci. 24 (8), 1351–1369. doi:10.1016/0009-2509(69)85055-4.

List of World's Polysilicon Producers According to Country for Last 3. (2013). https://studylib.net/doc/8255119/list-of-world-s-polysilicon-producers-according-to-countr.

Martín, M, 2016. Industrial Chemical process. Industrial Chemical Process. Analysis and Design. Elsevier, Oxford.

Morita, K., Yoshikawa, T., 2011. Thermodynamic evaluation of new metallurgical refining processes for SOG-silicon production. Trans. Nonferrous Metals Soc. China 21 (3), 685–690. doi:10.1016/S1003-6326(11)60766-8.

Muller, D., Ronge, G., Fer, J.S., Leimkuhler, H.J., 2002. Development and economic evaluation of a reactive distillation process for silane production. In Proc. Int. Conf. Distill. Absorp. pp. 4-1.

National Institute of Standards and Technology (NIST), 2018. Libro del Web de Química del NIST. U.S. Department of Commerce. Recovered from. https://webbook.nist.gov/chemistry/.

Ni, H., Lu, S., Chen, C., 2014. Modeling and simulation of silicon epitaxial growth in Siemens CVD reactor. J. Cryst. Growth 404, 89–99. doi:10.1016/j.jcrysgro.2014.07.006.

Nie, Z., Ramachandran, P.A., Hou, Y., 2018. Optimization of effective parameters on Siemens reactor to achieve potential maximum deposition radius: An energy consumption analysis and numerical simulation. Int. J. Heat Mass Transf. 117, 1083–1098. doi:10.1016/j.ijheatmasstransfer.2017.10.084.

O'Mara, W., Herring, R.B., Hunt, L.P., 2007. Handbook of semiconductor silicon technology. Crest Publishing House.

Payo, M.J.R., 2008. Purificación de triclorosilano por destilación en el proceso de obtención de silicio de grado solar. Universidad Complutense de Madrid Doctoral dissertation.

Pazzaglia, G., Fumagalli, M., &Kulkarni, M. (2011). *U.S. Patent Application* No. 13/084,243.

Pizzini, S., 2010. Towards solar grade silicon: Challenges and benefits for low cost photovoltaics. Solar Energy Mater. Solar Cells 94 (9), 1528–1533. doi:10.1016/j.solmat.2010.01.016.

Polman, A., Knight, M., Garnett, E.C., Ehrler, B., Sinke, W.C., 2016. Photovoltaic materials: Present efficiencies and future challenges. Science 352 (6283). doi:10.1126/science.aad4424, aad4424.

PVinsights, 2019. PVinsights Grid the world.United States of America Publishing. Recovered from. http://pvinsights.com/.

Ramírez-Márquez, C., Contreras-Zarazúa, G., Martín, M., Segovia-Hernández, J.G., 2019. Safety, Economic, and Environmental Optimization Applied to Three Processes for the Production of Solar-Grade Silicon. ACS Sustain. Chem. Eng. 7 (5), 5355–5366. doi:10.1021/acssuschemeng.8b06375.

Ramírez-Márquez, C., Otero, M.V., Vázquez-Castillo, J.A., Martín, M., Segovia-Hernández, J.G., 2018. Process design and intensification for the production of solar grade silicon. J. Clean. Prod. 170, 1579–1593. doi:10.1016/j.jclepro.2017.09.126.

Ramírez-Márquez, C., Sánchez-Ramírez, E., Quiroz-Ramírez, J.J., Gómez-Castro, F.I., Ramírez-Corona, N., Cervantes-Jauregui, J.A., Segovia-Hernández, J.G., 2016. Dynamic behavior of a multi-tasking reactive distillation column for production of silane, dichlorosilane and monochlorosilane. Chem. Eng. Process. Process Intens. 108, 125–138. doi:10.1016/j.cep.2016.08.005.

Ramos, A., Filtvedt, W.O., Lindholm, D., Ramachandran, P.A., Rodríguez, A., Del Cañizo, C., 2015. Deposition reactors for solar grade silicon: A comparative thermal analysis of a Siemens reactor and a fluidized bed reactor. J. Cryst. Growth 431, 1–9.

Ranjan, S., Balaji, S., Panella, R.A., Ydstie, B.E., 2011. Silicon solar cell production. Comp. Chem. Eng. 35 (8), 1439–1453. doi:10.1016/j.compchemeng.2011.04.017.

Schweidtmann, A.M., Huster, W.R., Lüthje, J.T., Mitsos, A., 2019. Deterministic global process optimization: Accurate (single-species) properties via artificial neural networks. Comp. Chem. Eng. 121, 67–74. doi:10.1016/j.compchemeng.2018.10.007.

Sugiura, M., Kurita, H., Nisida, T., Fuwa, A., 1992. Hydrogenation Reactions and Their Kinetics for SiCl4 (g)–H2 (g) and SiCl4 (g)–Si (s)–H2 (g) Systems Using a Fixed Bed Type Reactor. Materials Transactions. JIM 33 (12), 1138–1148. doi:10.2320/matertrans1989.33.1138.

Turton, R., Bailie, R.C., Whiting, W.B., Shaeiwitz, J.A., Bhattacharyya, D., 2012. Analysis, Synthesis and Design of Chemical Processes. Pearson Education.

Voutchkov, I. and Keane, A.J. (2006) Multiobjective optimization using surrogates. Adaptive Computing in Design and Manufacture 2006 (ACDM 2006). 25 - 27 Apr 2006. pp. 167-175.

Union Carbide, 1981. Base Gas Condition for use Silane Process. Report DOE/JPL-954343-21, Nat. Tech. Inform.. Center, Springfield, VA.

Wai, C.M., Hutchison, S.G., 1989. Free energy minimization calculation of complex chemical equilibria: Reduction of silicon dioxide with carbon at high temperature. J. Chem. Educ. 66 (7), 546. doi:10.1021/ed066p546.

Wang, C., Wang, T., Li, P., Wang, Z., 2013. Recycling of SiCl4 in the manufacture of granular polysilicon in a fluidized bed reactor. Chem. Eng. J. 220, 81–88. doi:10.1016/j.cej.2013.01.001.

Walas, S.M., 1990. Chemical Process Equipment: Selection and Design. Butterworth-Heinemann.

Wang, X., 2011. Two-Dimensional Temperature Distribution in Fluidized Bed Reactors for Synthesizing Trichlorosilane (Doctoral dissertation. Hong Kong Univ. Sci. Tech..

Weber, K.J., Blakers, A.W., Stocks, M.J., Babaei, J.H., Everett, V.A., Neuendorf, A.J., Verlinden, P.J., 2004. A novel low-cost, high-efficiency micromachined silicon solar cell. IEEE Electron Device Lett. 25 (1), 37–39. doi:10.1109/LED.2003.821600.

Yadav, S., Chattopadhyay, K., Singh, C.V., 2017. Solar grade silicon production: A review of kinetic, thermodynamic and fluid dynamics based continuum scale modeling. Renew. Sustain. Energy Rev. 78, 1288–1314. doi:10.1016/j.rser.2017.05.019.

Zadde, V.V., Pinov, A.B., Strebkov, D.S., Belov, E.P., Efimov, N.K., Lebedev, E.N., … Touryan, K., 2002. New method of solar grade silicon production. *12th Workshop on Crystalline Silicon Solar Cell Materials and Processes: Extended Abstracts and Papers from the workshop held 11-14 August 2002, Breckenridge, Colorado (No. NREL/CP-520-35650)*.National Renewable Energy Lab..